

České vysoké učení technické v Praze
Fakulta jaderná a fyzikálně inženýrská

Czech Technical University in Prague
Faculty of Nuclear Sciences and Physical Engineering

Doc. Dr. Ing. Petr Haušild

**URČOVÁNÍ VLASTNOSTÍ JEDNOTLIVÝCH FÁZÍ Z DAT
NAMĚŘENÝCH MATICOVOU INDENTACÍ**

**DETERMINATION OF THE INDIVIDUAL PHASE
PROPERTIES FROM THE MEASURED GRID INDENTATION
DATA**

Summary

Statistical distribution of grid indentation data measured in multiphase materials can be significantly affected by the presence of an interface between adjacent materials. Generally, the experimental conditions choice is made such that the indentation depth is lower than a critical indentation depth below which microstructural length scales do not interfere significantly with the indentation response, and hence the indentation data acquired to such a depth provide access to the intrinsic properties of the material. Nevertheless, the indentation in proximity of the interface cannot always be completely avoided – in the grid indentation, the position of some indents can coincide with the phase boundary, or the invisible phase boundary can be close below the indenter contact area.

The influence of an interface on the distribution of measured indentation moduli was therefore characterized in model metal-metal, ceramic-ceramic and metal-ceramic composites. The change of properties near the interface was simulated by finite element method and experimentally verified by indentation in proximity of the boundary between two phases with distinctly different mechanical properties varying the depth of penetration and the distance from the interface. Subsequently, the conditional probability of measuring near the interface was quantified by beta distribution function with parameters dependent on the size of the volume/area affected by the presence of the interface. Using this approach, the intrinsic properties of the individual materials were successfully extracted from the experimental grid indentation data.

Souhrn

Výsledky naměřené maticovou indentací ve vícefázových materiálech mohou být významně ovlivněny přítomností rozhraní mezi sousedními materiály. Obvykle se podmínky experimentu volí tak, aby hloubka vtisku byla menší než určitá kritická hodnota, pod kterou není indentační odezva ovlivněna mikrostrukturou. Tato kritická hodnota závisí na vlastnostech (modulu, tvrdosti...) i geometrii (velikosti a tvaru částic...) jednotlivých fází. V některých případech však nelze zcela zamezit indentací v blízkosti rozhraní – při maticové indentaci může poloha některých vtisků koincidovat s fázovým rozhraním, nebo může být neviditelné fázové rozhraní skryto pod povrchem v blízkosti oblasti kontaktu.

Vliv hodnot měřených v blízkosti rozhraní na celkovou distribuci naměřených hodnot (Youngova modulu, tvrdosti) byl charakterizován v modelových kompozitech kov-kov, kov-keramika a keramika-keramika. Ovlivnění vlastností u rozhraní bylo numericky simulováno metodou konečných prvků a experimentálně charakterizováno indentací v blízkosti rozhraní mezi dvěma materiály s odlišnými vlastnostmi. Indentace byla provedena v různých vzdálenostech od rozhraní a do různé hloubky. Následně byla podmíněná pravděpodobnost měření (pro danou hloubku vtisku) v blízkosti rozhraní proložena beta distribuční funkcí s parametry závislými na objemovém podílu ovlivněném přítomností rozhraní. Tento postup umožnil identifikaci (intrinsických) vlastností jednotlivých fází z dat naměřených maticovou indentací.

Klíčová slova

Nanoindentace; instrumentovaná indentace; maticová indentace; rozhraní; tvrdost; Youngův modul; kompozity

Keywords

Nano-indentation; instrumented indentation; grid indentation; interface; hardness; Young modulus; composites

CONTENTS

1. Introduction	6
2. Theoretical background	11
3. Validation methodology	17
3.1 Experimental details	17
2.2 FEM analysis	20
4. Results and discussion	23
4.1 Indentation across the interface	23
4.2 Grid indentation	27
5. Conclusions	30
References	31
Curriculum vitae	34

1. Introduction

Instrumented (depth-sensing) indentation is extensively used nowadays for the characterization of local mechanical properties of various materials including metals, ceramics, polymers or composites [1]. This method can be performed on very small and/or thin specimens by applying very small loads resulting in depths at the nanometer scale [2]. The principal goal of this method is to extract hardness and Young's modulus from the indenter load vs. depth of penetration profile (Fig. 1). The most commonly used method is the Oliver and Pharr method [3,4] which forms the basis for the instrumented indentation testing standard (ISO 14577 [5]).

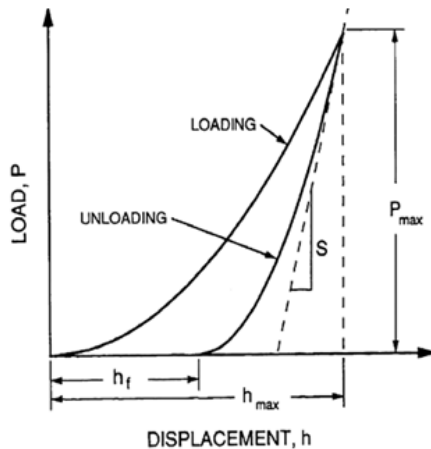


Fig. 1 Schematic illustration of indentation load-displacement data [3].

This procedure is founded upon elastic solution of contact problem (Sneddon's solution [6]). An underlying assumption of this method is that the indented solid body is homogeneous and isotropic. When indenting in proximity of an interface between two phases with different properties, this assumption is no longer valid. However, the instrumented indentation of structurally heterogeneous materials using Oliver-Pharr method is frequently employed in order to characterize the properties of individual phases as this method is simple and available in practically all commercial devices.

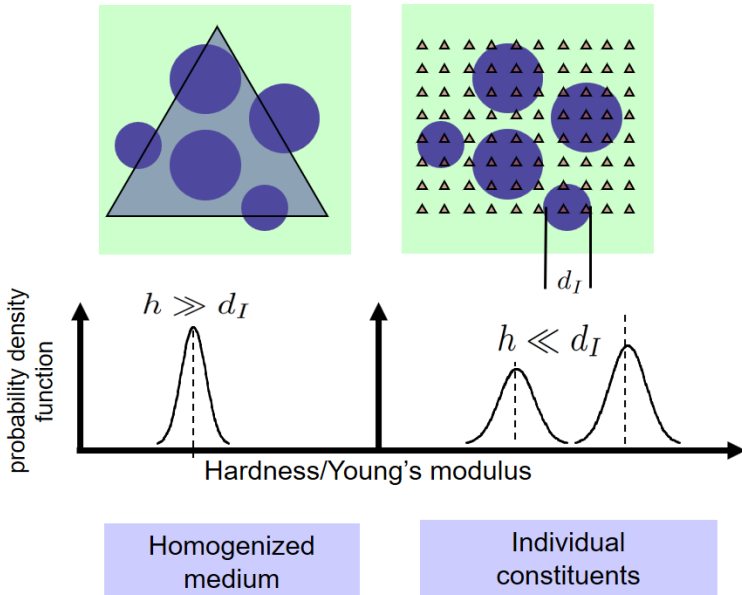


Fig. 2 Schematic illustration of grid indentation at different length scale [8].

One way of characterizing the microstructurally heterogeneous materials is the positioning of *isolated* indentations (e.g. with the aid of light microscopy) inside the individual phases, sufficiently far from the interface, which permits to obtain the properties of single phases. Another way is the *grid indentation* which is based on performing a large number of equidistantly spaced indentations and their statistical evaluation [7,8]. Both methods need the knowledge of so called indentation length scale since it has been shown many times that the particle size, shape and properties do influence the indentation response (see Fig. 2). Generally, the experimental conditions choice is made such that the indentation depth is lower than a critical indentation depth below which microstructural length scales do not interfere significantly with the indentation response, and hence the indentation data acquired to such a depth provide access to the intrinsic properties of the material. Nevertheless, the indentation in proximity of the interface cannot always be completely avoided – in the grid indentation, the position of some

indents can coincide with the phase boundary, or the invisible phase boundary can be close below the indenter contact area (Fig. 3), which can by the way occur for both grid and isolated indentations.



Fig. 3 Schematic illustration of indentation in proximity of the interface hidden below the indenter contact area.

An often-used rule of thumb limits the maximum indentation depth to one tenth of the film thickness. In two-phase materials, a similar depth limit can be defined by dividing the contact radius with the particle radius [9]. However, a critical indentation depth with respect to the size of the heterogeneity depends also on the phase geometry and modulus (and other mechanical properties) mismatch (see Fig. 4).

For the isolated indentation, the load vs. depth of penetration curves which show a transition from characteristic soft to hard loading behavior (and vice versa), should be excluded from the analysis [7,9].

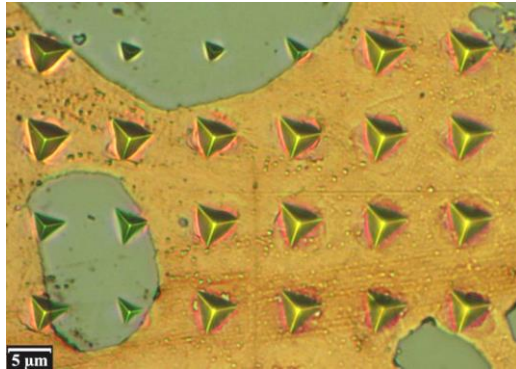


Fig. 4 Grid indentation in two-phase material (tungsten-copper) showing the effect of the presence of the interface on the size of indents.

For the grid indentation technique, it is frequently much more difficult to exclude all the influenced measurements. When applying the statistical evaluation of results, e.g. a bimodal Gaussian fit, the presence of boundary-affected results leads to the bias of the distribution, i.e. to an overestimation of the softer phase hardness and/or modulus together with an underestimation of harder phase values [10]. Some improvements were achieved taking an interface as an “extra” phase with a flat Gaussian distribution [11]. However, this is not correct as the change of materials behavior definitely does not follow the Gaussian distribution. Moreover, it leads to three more parameters, which exceedingly complicates the identification procedure as it necessitates huge amount of data.

The aim of this work is to present a case study on two-phase materials with distinctly different hardness and Young’s modulus. The influence of depth of penetration and microstructural length scale on the measured indentation modulus or hardness distribution was incorporated via presence of transitional zone with a progressive change of materials behavior (Fig. 5).

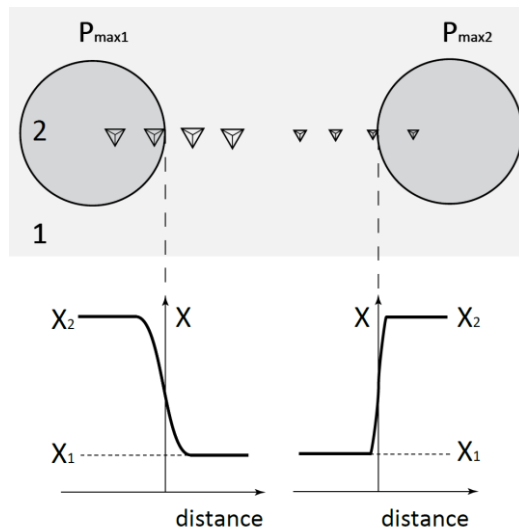


Fig. 5 Schematic illustration of the transition from hard to soft or soft to hard behavior when indenting across the interface between phases 1 and 2 with unlike property X (E or H) using different loads P_{\max} .

The probability of indentation in the affected area as a function of depth of penetration and size of particles was simulated by finite element computations and fitted by a statistical distribution function. Subsequently, this approach was experimentally verified by indentation in proximity of the boundary between the phases with distinctly different mechanical properties. Finally, the intrinsic properties of the material were successfully extracted from the experimental grid indentation data.

2. Theoretical background

When indenting near the interface between two phases with different properties, the measured values (hardness or Young's modulus) can be affected by two principal factors. The first factor can be associated with the material property, the second one with the experimental method. In order to understand the effect of an interface on the distribution of measured indentation data, it is convenient to briefly summarize the idealized cases.

The first case corresponds to measuring with “ideal” indenter (with point contact, affecting infinitesimally small volume under the indenter, and introducing no scatter to the evaluation method) on a composite of two “ideal” materials (with no scatter in material properties). The obtained cumulative distribution function (CDF) is then characterized by two jump discontinuities at properties 1 and 2 (i.e. Heaviside step functions), and probability density function (pdf) involves two Dirac delta functions as can be illustrated e.g. for Young's modulus in Fig. 6 and Eq. 1:

$$pdf(E) = p_1\delta(E_1) + p_2\delta(E_2) \quad (1)$$

where p_1 and p_2 are the volume/area fraction of the phase 1 and 2 respectively ($p_1+p_2=1$), E_1 and E_2 are the Young's moduli of the phase 1 and 2 respectively.

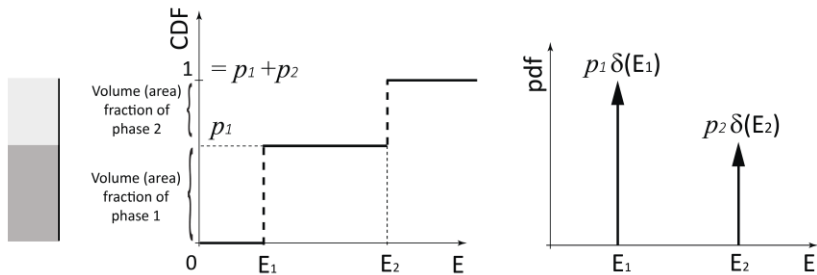


Fig. 6 Schematic illustration of the (apparent) Young's modulus distribution when measuring with infinitesimally small indents in material with “ideal” phase properties.

In the next case, all conditions are the same (no scatter in material properties and/or in experimental method), except the fact that the stress field induced by the indentation affects the volume under and next to the contact area. Measurement across the boundary between two phases therefore depends on the size (depth) of the indent as it is illustrated in Fig. 5. The cumulative distribution function must then incorporate this S-shape transition from one material property to the other in the volume/area fraction affected by the presence of the interface. In the limiting case when the volume/area fraction affected by the presence of the interface approaches to zero, the distribution shall tend to precedent case.

These conditions are effectively fulfilled by using the beta distribution with the probability density function:

$$pdf(x) = \frac{x^{a-1}(1-x)^{b-1}}{B(a,b)} \quad (2)$$

which is defined for x from the interval $<0,1>$, the shape parameters a and b are from the interval $<0,1>$ to ensure the U-shape of the probability density function (Fig 2b). When the parameters $a \rightarrow 1$ and $b \rightarrow 1$, this probability density function tends to that of uniform distribution. Decreasing parameters a and b lead to narrower transition from one material property to the other (i.e. decrease of the volume/area fraction affected by the presence of the interface as shown in Fig 7). When the parameters $a \rightarrow 0$ and $b \rightarrow 0$, the probability density function tends to two Dirac delta functions. Normalization constant $B(a,b)$ is given by the beta function (Euler integral of the first kind):

$$B(a,b) = \int_0^1 x^{a-1}(1-x)^{b-1} dx \quad (3)$$

It will be shown later that the change of materials behavior measured by indentation across the interface can effectively be approximated by inverse beta distribution, so that the (normalized) measured values can be statistically described by:

$$pdf(E) = \frac{\left(\frac{E - E_1}{E_2 - E_1}\right)^{a-1} \left(1 - \frac{E - E_1}{E_2 - E_1}\right)^{b-1}}{(E_2 - E_1)B(a, b)} \quad (4)$$

for $E_1 < E_2$, $E \in (E_1, E_2)$, elsewhere $pdf(E) = 0$.

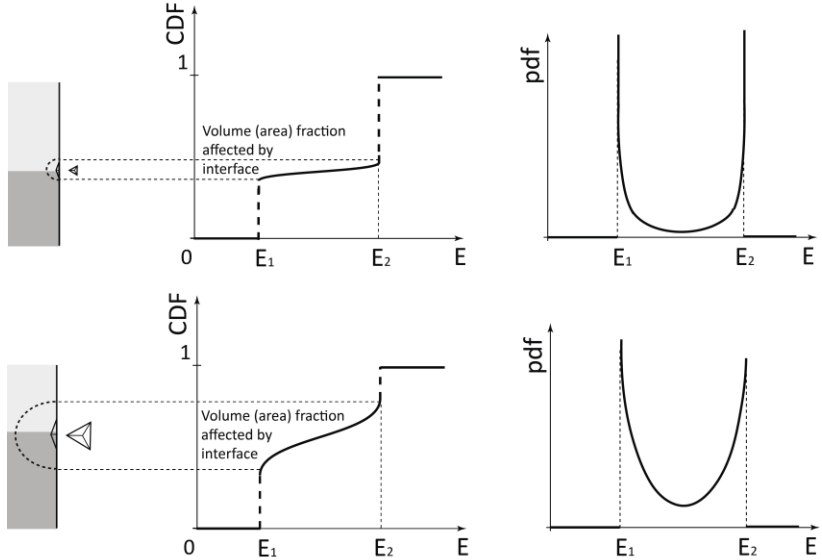


Fig. 7 Schematic illustration of the (apparent) Young's modulus distribution when measuring with indents of different (finite) size in material with "ideal" phase properties.

In the third case, measuring indenter with point contact and affecting infinitesimally small volume under the indenter is assumed, however, scatter in material properties of both phases can be introduced e.g. by different crystallographic orientation (see Fig. 8) [12-15], state of the surface or e.g. by the experimental device [16,17].

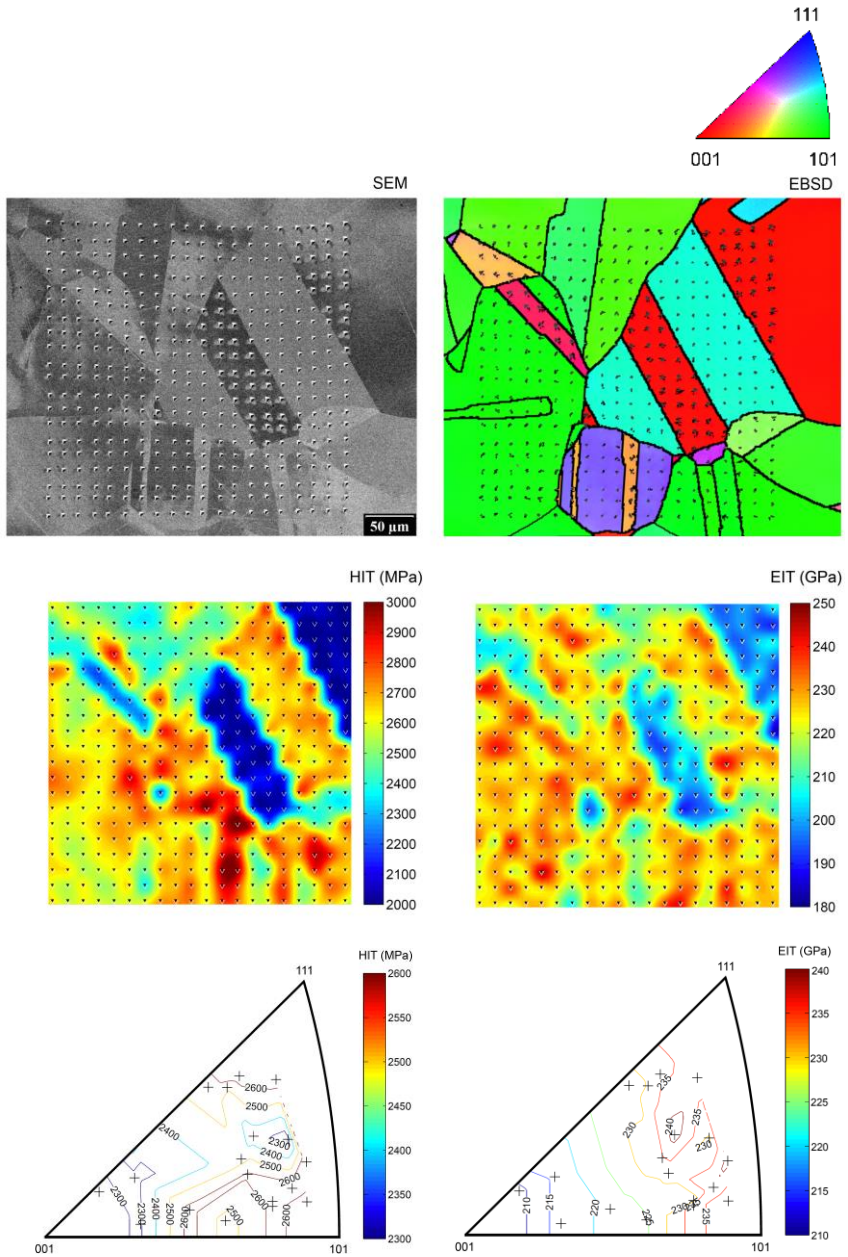


Fig. 8 Anisotropy of hardness and Young's modulus in A304 stainless steel revealed by grid indentation [14].

The obtained (bimodal) distribution can be then mixed from two Gaussian distribution.

$$pdf(E) = \frac{p_1}{\sqrt{2\pi}\sigma_1} \exp\left[-\frac{(E - \bar{E}_1)^2}{2\sigma_1^2}\right] + \frac{p_2}{\sqrt{2\pi}\sigma_2} \exp\left[-\frac{(E - \bar{E}_2)^2}{2\sigma_2^2}\right] \quad (5)$$

where parameters \bar{E}_1 , \bar{E}_2 represent mean values of Young's moduli and the σ_1 , σ_2 scatter of Young's moduli in the phases 1 and 2.

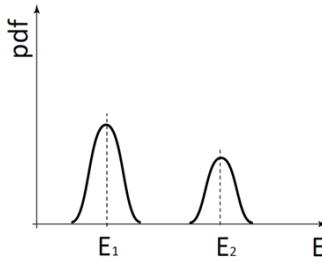


Fig. 9 Schematic illustration of the (apparent) Young's modulus distribution in material exhibiting scatter in individual phase properties.

Combining the second and third case, i.e. assuming the “real” indenter (of finite size) and scattered material properties, the resulting data distribution is given by conditional probability of measuring in phase 1, 2 or near the interface between phase 1 (with actual material property 1) and phase 2 (with actual material property 2):

$$\begin{aligned}
pdf(E) = & \frac{p_1}{\sqrt{2\pi}\sigma_1} \exp\left[-\frac{(E - \bar{E}_1)^2}{2\sigma_1^2}\right] \\
& + \frac{p_2}{\sqrt{2\pi}\sigma_2} \exp\left[-\frac{(E - \bar{E}_2)^2}{2\sigma_2^2}\right] \\
& + p_3 \int_{-\infty}^{+\infty} \int_{-\infty}^{+\infty} \frac{\left(\frac{E - E_1}{E_2 - E_1}\right)^{a-1} \left(1 - \frac{E - E_1}{E_2 - E_1}\right)^{b-1}}{(E_2 - E_1)B(a, b)} \cdot \\
& \cdot \frac{1}{\sqrt{2\pi}\sigma_1} \exp\left[-\frac{(E_1 - \bar{E}_1)^2}{2\sigma_1^2}\right] \cdot \\
& \cdot \frac{1}{\sqrt{2\pi}\sigma_2} \exp\left[-\frac{(E_2 - \bar{E}_2)^2}{2\sigma_2^2}\right] dE_1 dE_2
\end{aligned} \tag{6}$$

where p_3 is the volume/area fraction affected by the presence of the interface, other parameters were explained in previous equations.

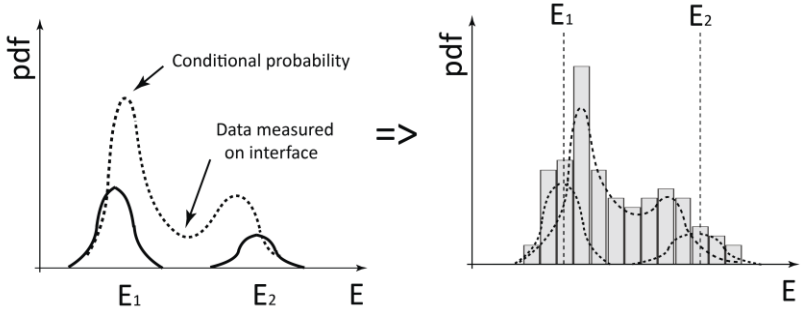


Fig. 10 Schematic illustration of the (apparent) Young's modulus distribution when measuring with indents of different (finite) size in material with "actual" phase property distribution.

This case is closest to the reality and will be considered in the following paragraphs.

3. Validation methodology

3.1 Experimental details

The samples chosen for this case study were two-phase composites with different combinations of materials: metal-metal (tungsten-copper, tungsten-SS410 steel), ceramic-ceramic (yttria-stabilized zirconia, YSZ- Al_2O_3) and metal-ceramic ($\text{FeAl-Al}_2\text{O}_3$). In all these composites, both constituents have distinctly different Young's modulus (about two times) and distinctly different hardness. The selected materials do not present important pile-up phenomenon and can therefore be advantageously characterized using Oliver and Pharr method.

Cylindrical samples were prepared by spark plasma sintering at the Institute of Plasma Physics from (commercially supplied) pure powders: under optimized conditions in order to obtain minimum porosity and to prevent the formation of any interlayer at the interface between the parent phases as e.g. the Fe_7W_6 intermetallic compounds in the case of W-steel composite.

The sample surfaces were subsequently ground and polished with final step in $0.05 \mu\text{m}$ non-crystallizing amorphous colloidal silica suspension to avoid the surface layer affected by mechanical grinding and polishing. Nanoindentation measurements were performed on Anton Paar CSM NHT Nanoindentation Tester with Berkovich indenter. The results were evaluated according to Oliver and Pharr method [3,4]. In this method, the unloading (i.e. elastic) part of load-displacement data is fitted by power law:

$$P = \alpha(h - h_f)^m \quad (7)$$

where P is the load, h is the depth, h_f is the final depth after unloading, α and m are parameters fitted by least square method.

The slope of the tangent to the data at maximum load dP/dh is then determined and inserted into Eq. (8) to give the contact depth h_c :

$$h_c = h_{\max} - \varepsilon \frac{P_{\max}}{dP / dh} \quad (8)$$

where the geometric constant ε is given for the conical indenter by $\varepsilon=2(\pi-2)/\pi \sim 0.72$ (for flat punch $\varepsilon=1$, and for the paraboloid of revolution $\varepsilon=0.75$) [18].

The contact area A is then found from the geometry of the indenter as a function of the contact depth h_c using formula:

$$A = C_0 h_c^2 + C_1 h_c + C_2 h_c^{1/2} + C_3 h_c^{1/4} + \dots + C_8 h_c^{1/128} \quad (9)$$

proposed in Ref. [3] and recommended by the standard [5]. The coefficients of the area function $C_0 \dots C_8$ were determined by calibration on material with known Young's modulus (fused silica). The indentation hardness H_{IT} , and the reduced modulus E^* can be then calculated as:

$$H_{IT} = \frac{P_{\max}}{A} \quad (10)$$

$$E^* = \frac{\sqrt{\pi}}{2\beta\sqrt{A}} \frac{dP}{dh} \quad (11)$$

where β is dimensionless correction factor applied since the elastic recovery of material upon removal of load leads to some significant deviations in the expected shape of the unloading portion of the load-displacement curve [19].

The reduced modulus E^* is related to Young's moduli of the specimen (E) and the indenter (E_i) by:

$$\frac{1}{E^*} = \frac{(1-\nu^2)}{E} + \frac{(1-\nu_i^2)}{E_i} \quad (12)$$

where ν and ν_i are Poisson's ratios of the specimen and the indenter respectively.

So-called continuous multicycle (CMC) indentations consisting in progressive loading with partial unloading were used to obtain indentation modulus for different loads (from different depths) at the same positions. The indentation parameters were chosen from preliminary experiments (single indentations at maximum load) in order to fulfill the conditions: i) cover sufficiently the area containing both phases, ii) do not influence other measurements (i.e. keep the distance between the indents at least at 3 times the size of final imprints).

First, the indentations were performed in known distances from the interface. For W-steel composite, the sample with a sharp interface oriented parallel to the surface normal (indenter axis) was prepared (both materials have practically the same Poisson's ratio and moderately different coefficients of thermal expansion, which resulted in good bonding along the interface). In the case of metal-ceramic and ceramic-ceramic composites, such sharp interface is hard (or impossible) to produce, so the indentations were performed near the particle boundaries (it should be noted that the interfaces under the surface were not necessarily oriented parallel to the indenter axis).

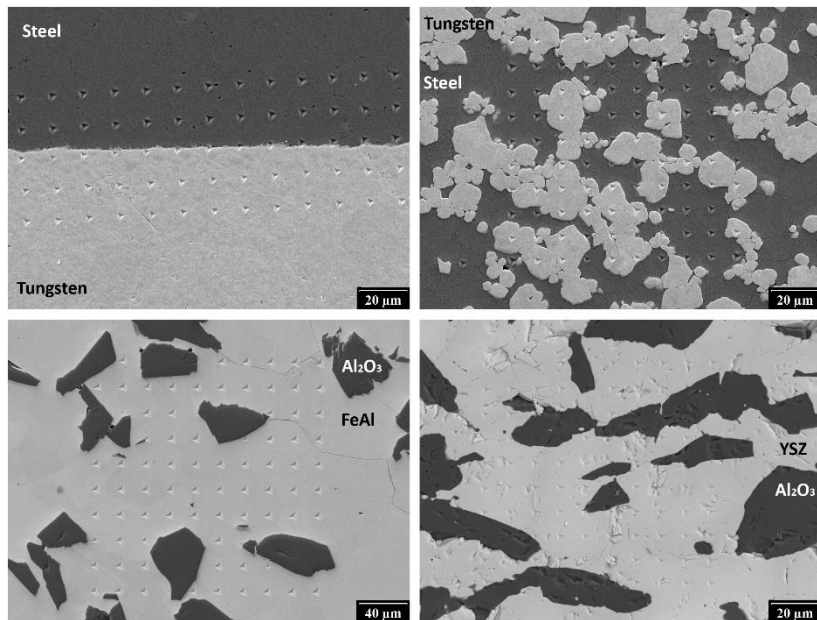


Fig. 11 SEM micrographs showing examples of grid indentations matrices in composites under the study [22].

Next, several matrices of (10x10, 10x20 or 20x20) equidistantly spaced CMC indentations (of 4-6 load levels) were performed on rectangular areas of dimensions varying in dependence of the size of composite phases.

After the indentations, the areas were examined with the aid of light microscope Neophot 32 and scanning electron microscope (SEM) JEOL JSM 5510LV. The matrices of indentations are illustrated in Fig. 11, where the microstructures are also shown.

The measured indentation moduli are presented in the form of plain strain indentation modulus to eliminate the effect of (a priori unknown) different Poisson's ratios of the analyzed phases:

$$E_{IT}^* = E_{IT} / (1 - \nu^2) \quad (13)$$

2.2 FEM analysis

Forward FEM analyses were carried out in MSC.Marc 2012 FEM code [20] to evaluate the effect of an interface on the apparent (measured) material property. For the evaluation of simulated load-displacement curves we adopted the method described above. Positions of interface versus indenter as well as the mesh geometry in the contact domain are illustrated in Fig. 12. For the modeling of Berkovich indenter we used an equivalent conical indenter with a half-apical angle of 70.3° [18]. The indenter was modeled by a rigid contact surface (with no friction). Elasticity in the indenter was neglected since it is important only for very hard materials (comparable to diamond).

Simulations were carried out using elastic and elastic-plastic material formulation. For the elastic-plastic task, the stress σ for $\sigma > \sigma_y$ was defined as:

$$\sigma = \sigma_y \left(1 + \frac{E}{\sigma_y} \varepsilon_p \right)^n \quad (14)$$

where ε_p is plastic strain, σ_y is (0.2% offset) yield strength and n is a strain-hardening exponent. Material parameters used in the elastic and elastic-plastic simulations were taken from Ref. [21] (see Table I).

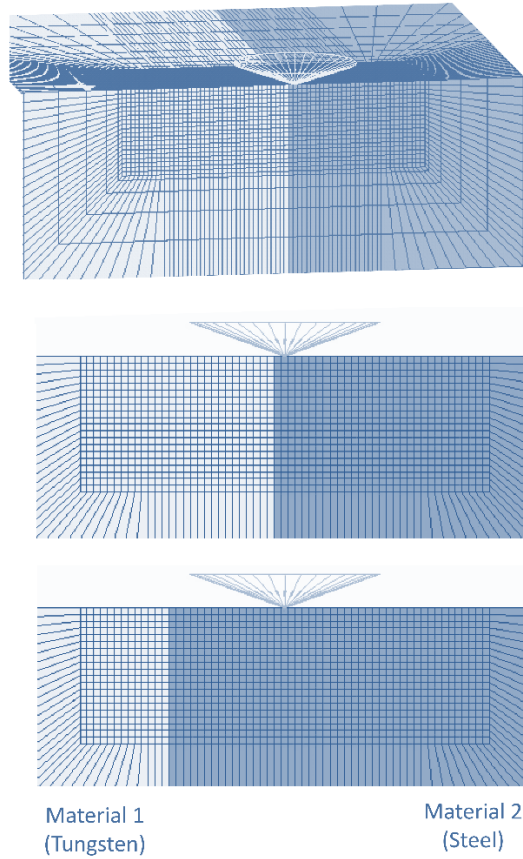


Fig. 12 Schematic sketch of the FEM mesh in the contact domain showing the position of the indenter with respect to the interface between two phases [22].

Table I. Material properties used in the elastic and elastic-plastic FEM simulations [21].

	E [GPa]	ν	σ_y [MPa]	n
Steel	210	0.3	682	0.17
Tungsten	406	0.3	794	0.23

The first half of unloading part of the load–displacement curve was fitted by the power-law model in the form of Eq. (7). The derivative of P – h curve at the point of maximum load dP/dh served as a direct input for computation of indentation moduli using Eq. (11), where correction factor β was set to 1.067 (the same value as obtained by Hay et al. [19]) according to simulation with isotropic material so that the contact area A could be directly derived from the conical geometry of the indenter:

$$A = \pi(h_c \tan 70.3^\circ)^2 \quad (15)$$

The contact depth h_c was evaluated using Eq. (8), supposing $\varepsilon = 0.72$.

4. Results and discussion

4.1 Indentation across the interface

Results of indentations with different positions of interface versus indenter simulated by FEM are shown in Fig. 12. It can be seen that in the case of simulations with elastic formulation, the self-similar nature of the task enables the normalization of distance from the interface by contact depth x/h_c . The change of indentation modulus measured by indentation across the interface can then be well approximated by symmetrical inverse beta distribution. The elastic-plastic simulations of indentations (using material parameters listed in previous section) lead to only slight deviation from the (symmetrical) inverse beta distribution fit. To note is also the fact that for $x/h_c > 10$ the effect of interface has completely vanished. The “interface affected region” is only slightly larger in the case of elastic-plastic materials than in elastic ones.

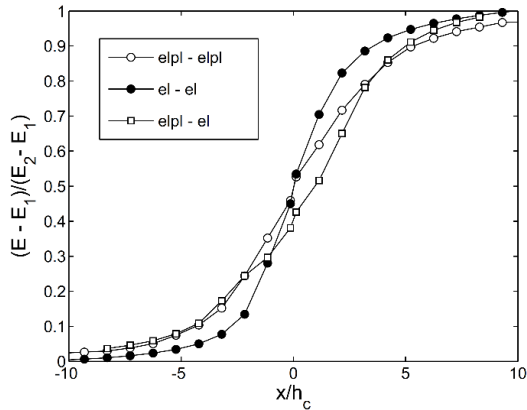


Fig. 12 The change of normalized indentation modulus computed by FEM across the interface between elastic/elastic, elastic-plastic/elastic-plastic and elastic/elastic-plastic materials as a function of normalized distance from the interface [22].

The most “severe” situation is the combination of soft plastic and hard elastic materials on each side of the interface (this can occur e.g. in the case of ceramic particles reinforced metal matrix composites such as Al-

Al₂O₃). However, even in the elastic/elastic-plastic case the approximation by (non-symmetrical) inverse beta distribution seems to be reasonable (at least for the material parameters from Table I). Unfortunately, it is hard to relate directly the parameters of non-symmetrical inverse beta distribution to hardness or indentation modulus of parent phases as they depend on overall material behavior in rather complex way (E , σ_y , n , $E/\sigma_y \dots$).

As a first approximation, it was therefore assumed that the results of experimental measurements across the interface can be assessed by symmetrical inverse beta distribution (with parameters $a=b$). First, the indentations on the W-steel sample with sharp interface oriented perpendicular to the surface of the sample and parallel to the indenter axis were performed. The indentation moduli measured by applying different loads in varying distances from the interface are shown in Fig. 13. It can be seen that for the same normalized distances x/h_c the measured values are not dependent on applied load, which is in agreement with the FEM simulations.

In the next step, the same experiments were carried out on particulate composites. In this case, the spatial orientation of the interface is a-priori unknown (not necessarily perpendicular to the surface and parallel to the indenter axis) and some part of particles can be hidden under the surface. Even if the previously developed model was built on the consideration of layered structure indented perpendicularly, the measured dependencies across the W-steel interface were very similar for the layered and particulate composites, and the sizes of zones influenced by presence of adjacent phase differed only very little.

The size of the transitional zone defined by distance at which 5% increase/decrease from the single phase indentation modulus mean values occurs was less than $20h_c$. In the case of metal-ceramic (FeAl-Al₂O₃) and ceramic-ceramic (YSZ-Al₂O₃) composites, the evolution of indentation modulus across the interface was only little steeper (the size of the transitional zone was less than $15h_c$) and the shape of the transition was quite similar (Fig. 13).

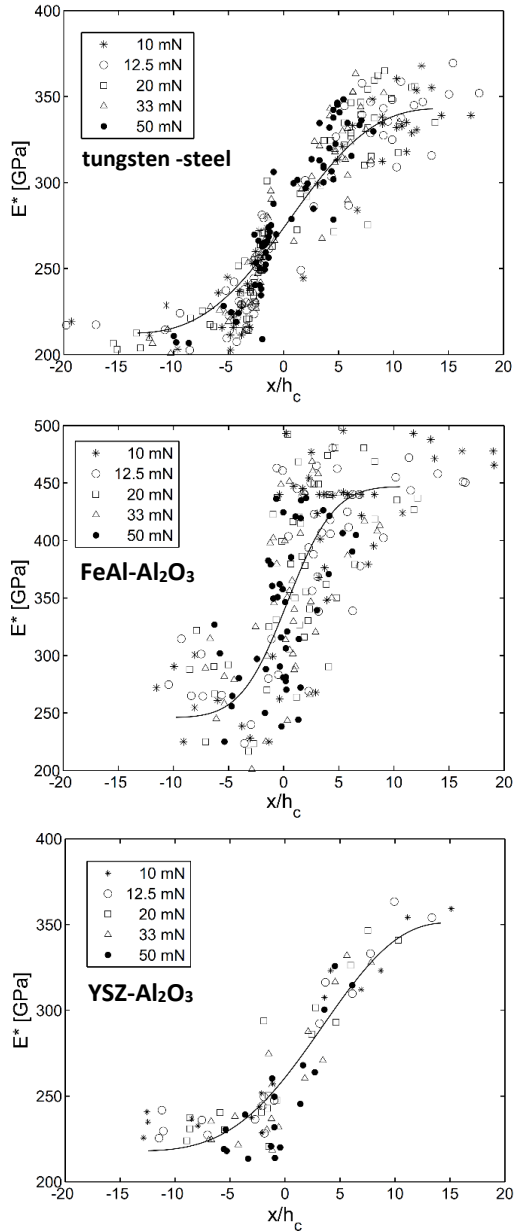


Fig. 13 The change of indentation modulus across the interface in metal-metal, metal-ceramic and ceramic-ceramic composites [22].

It is to note that so computed or experimentally obtained sizes of the transitional zones can serve for rough estimation of the area/volume fraction affected by the presence of interface for known microstructure (with known boundary length) and, therefore, for optimizing the choice of the penetration depth (maximum load) in the grid indentation. Nevertheless, as it has already been stated in previous sections, the indentation in proximity of the interface cannot be completely avoided as the surface roughness and particle size and shape impose limitations on the suitable depth of indentation.

The evolutions of indentation modulus across the interface obtained by FEM and/or experimentally were subsequently used to reproduce the interaction of real two-phase microstructure with the indentation at different load. By varying the range of x/h_c on which the inverse beta distribution fit was performed (i.e. the ratio between particle size and depth of indentation), the different area/volume fraction affected by the presence of interface can be simulated (Fig. 14). The dependence of fitted beta distribution parameter a ($=b$) on the size (resp. fraction) of the transition zone can be effectively fitted by exponential relation:

$$a = A[\exp(Bp_3) - 1] \quad (16)$$

Parameter A depends on the definition of the transitional zone size; region bounded by 5% increase/decrease from the single phase indentation modulus mean values yields value A of about 0.3. Parameter B was arbitrarily obtained by the boundary condition $a=1$ at $p_3=1$ (i.e. $B=\ln[1+1/A]$).

This choice of B corresponds to the assumption of integral averaging of composite overall indentation modulus distribution using Eq. (6). In the case of other rules of mixture (e.g. Voigt or Reuss models [23]), alternative value of B can be imposed. Nevertheless, it should be noted that for area/volume fractions affected by the presence of the interface substantially higher than area/volume fractions of pure phases this procedure loses sense as the actual aim of the methodology is to gain the parameters of pure phases, not to estimate the homogenized indentation modulus.

4.2 Grid indentation

Grid CMC indentations performed on different combinations of composites (metal-metal, ceramic-ceramic and metal-ceramic) allowed to statistically treat the results for each load level in order to obtain the increasing number of measured values affected by the interface. Examples of statistical distributions obtained for selected loads are shown in Fig. 15. For the sake of simplicity, the results are presented for indentation modulus only. The same findings can be obtained for hardness, but only if there is no indentation size effect for the whole load range (one must take care as the indentation size effect is generally much stronger for hardness than for indentation modulus).

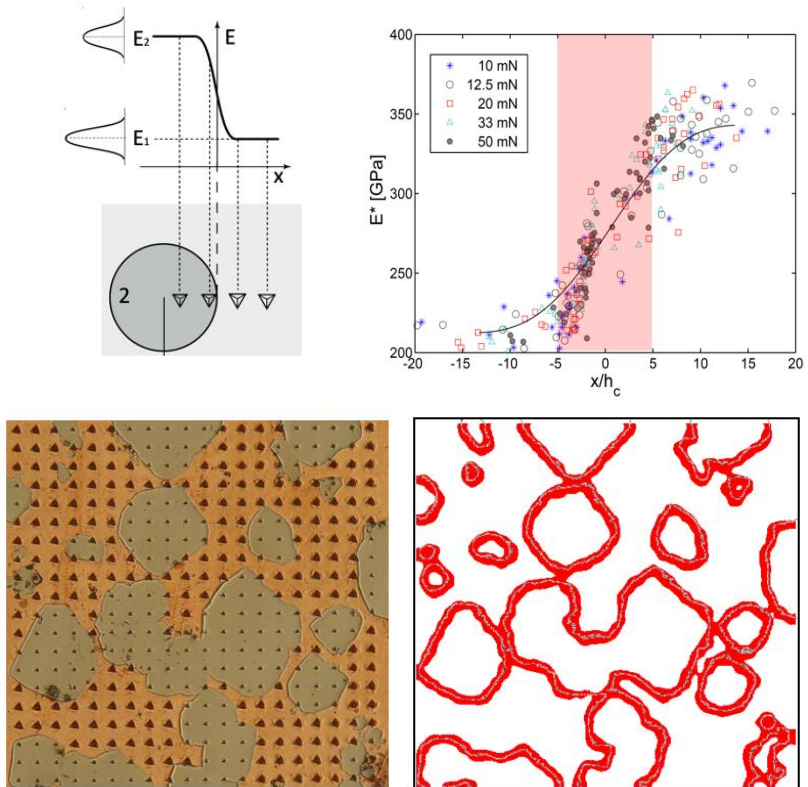


Fig. 14 Schematic illustration of the size of the area affected by the interface.

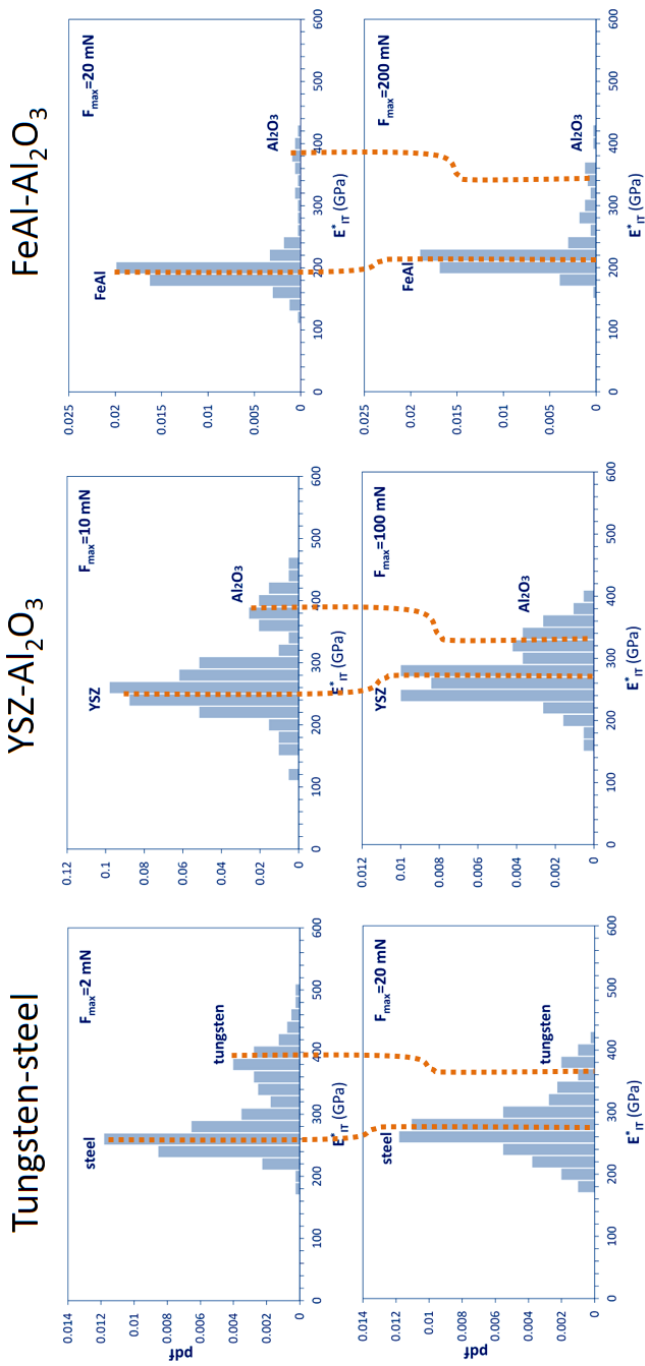


Fig. 15. Histograms of indentation moduli measured in W-steel, FeAl- Al_2O_3 and YSZ- Al_2O_3 composites at different loads.

It can be seen in Fig. 15 that the peaks of indentation moduli distribution are mutually shifted to one another as the indentation load (and/or depth of penetration) increases. It is obvious that indentation at significantly higher loads would lead only to averaged values of both phases.

First, the data were fitted by a Gaussian bimodal distribution (Eq. 5) using maximum likelihood method. Using Gaussian bimodal fit, Young's modulus of the softer phase is increasingly overestimated and the harder phase value is progressively underestimated. No clear trend could be seen in the identified volume fractions and the scatters associated with both phases, which is due to the fact that variation of these parameters only adjusts Gaussian bimodal distribution to non-Gaussian data (in order to obtain the best fit).

To overcome this drawback, the probability of indentation near the interface between phase 1 with actual material property 1 and phase 2 with actual material property 2 must be taken into account. Analyses performed in previous paragraphs reduced the number of additional parameters in Eq. 6 to one extra parameter only (volume/area fraction affected by the presence of the interface p_3) – see Eq. 16. Data fitting was performed using maximum likelihood method. Presence of the term taking into account the probability of indentation near the interface led to decrease of scatters associated with both phases and to identified values of indentation modulus consistent with the values of pure phases and probably better than those obtained by Gaussian bimodal fit for lowest indentation load.

The methodology can also be applied on a material containing relatively small particles, i.e. the case when measuring in the particles is very probably affected by the surrounding matrix. Several attempts have already been made in order to extract the properties of thin films [1,2] or hard particles embedded in soft matrix [9,27]. These methods were generally based on use of an exponential function to fit the indentation modulus measured at different indentation depths [1,2] or results obtained by FEM simulations [9,27]. Taking into account the presented configuration of the indentation across a particle (in comparison with e.g. soft to hard or hard to soft transition when indenting thin film), the use of

inverse beta distribution in combination with the grid indentation technique can be regarded as a useful extension of these methods.

5. Conclusions

The influence of presence of an interface on the distribution of measured indentation modulus was characterized in metal-metal, ceramic-ceramic and metal-ceramic composites prepared from pairs of pure powders by spark plasma sintering. The results can be summarized as follows:

- Determination of the individual phase properties from the measured grid indentation data using standard bimodal Gaussian fit leads to the softer phase indentation modulus overestimation together with the underestimation of the harder phase values due to the presence of boundary-affected results.
- The indentation in proximity of the interface cannot always be completely avoided – the position of some indents can coincide with the phase boundary, or the invisible phase boundary can be hidden close below the indenter contact area.
- To overcome this problem, the conditional probability of indentation near the interface between phase 1 (with actual material property 1) and phase 2 (with actual material property 2) has to be taken into account.
- The change of Young's (apparent) modulus measured by indentation across the interface can be well approximated by symmetrical inverse beta distribution. The parameters of beta distribution are connected with the area/volume fraction in which the indentation measurements are affected by the interface.
- Distribution incorporating conditional probability of indentation near the interface via beta distribution leads to values of identified Young's modulus much more consistent with the values of pure phases.

Main results presented in this text were published in Ref. [22] which is available at Springer via <http://dx.doi.org/10.1557/jmr.2016.375>

References

- [1] M.F. Doerner, and W.D. Nix: A method for interpreting the data from depth-sensing indentation instruments. *J. Mater. Res.* **1**, 601 (1986)
- [2] J. Menčík, D. Munz, E. Quandt, E.R. Weppelmann, and M.V. Swain: Determination of elastic-modulus of thin-layers using nanoindentation. *J. Mater. Res.* **12**, 2475 (1997)
- [3] W.C. Oliver, and G.M. Pharr: Improved technique for determining hardness and elastic modulus using load and displacement sensing indentation experiments. *J. Mater. Res.* **7**, 1564 (1992)
- [4] W.C. Oliver, and G.M. Pharr: Measurement of hardness and elastic modulus by instrumented indentation, Advances in understanding and refinements to methodology. *J. Mater. Res.* **19**, 3 (2004)
- [5] ISO 14577-2, Instrumented indentation test for hardness and materials parameters. (2002)
- [6] I.N. Sneddon: The relation between load and penetration in the axisymmetric Boussinesq problem for a punch of arbitrary profile. *Inter. J. Eng. Sci.* **3**, 47 (1965)
- [7] G. Constantinides, K.S. Ravi Chandran, F.-J. Ulm, and K.J. Van Vliet: Grid indentation analysis of composite microstructure and mechanics, Principles and validation. *Mater. Sci. Eng. A* **430**, 189 (2006)
- [8] N.X. Randall, M. Vandamme, and F.-J.Ulm: Nanoindentation analysis as a two-dimensional tool for mapping the mechanical properties of complex surfaces. *J. Mater. Res.* **24**, 679 (2009)
- [9] K. Durst, M. Göken, and H. Vehoff: Finite element study for nanoindentation measurements on two-phase materials. *J. Mater. Res.* **19**, 85-94 (2004)
- [10] P. Haušild, J. Nohava, and P. Pilvin: Characterisation of strain-induced martensite in a metastable austenitic stainless steel by nanoindentation. *Strain* **47**, 129 (2011)
- [11] J. Nohava, P. Haušild, Š. Houdková, and R. Enžl: Comparison of isolated indentation and grid indentation methods for HVOF sprayed cermets, *J. Therm. Spray Techn.* **21**, 651 (2012)
- [12] J.J. Vlassak, and W.D.Nix: Indentation modulus of elastically

- anisotropic half spaces. *Phil. Mag. A* **67**, 1045 (1993)
- [13] J.J. Vlassak, and W.D.Nix: Measuring the elastic properties of anisotropic materials by means of indentation experiments. *J. Mech. Phys. Solids* **42**, 1223 (1994)
- [14] P. Haušild, A. Materna, and J. Nohava: Characterization of anisotropy in hardness and indentation modulus by nanoindentation. *Metallogr. Microstruct. Anal.* **3**, 5 (2014)
- [15] A. Materna, P. Haušild, and J. Nohava: A numerical investigation of the effect of cubic crystals orientation on the indentation modulus. *Acta Physica Polonica A* **128**, 693 (2015)
- [16] J. Menčík, and M.V. Swain: Characterisation of materials using micro-indentation tests with pointed indenters. *Mater. Forum* **18**, 277 (1994)
- [17] J. Menčík, and M.V. Swain: Errors associated with depth-sensing microindentation tests. *J. Mater. Res.* **10**, 1491 (1995)
- [18] A.C. Fischer-Cripps: Nanoindentation. 3rd ed. Springer, New York (2011)
- [19] J.C. Hay, A. Bolshakov, and G.M. Pharr: A critical examination of the fundamental relations used in the analysis of nanoindentation data. *J. Mater. Res.* **14**, 2296 (1999)
- [20] Marc 2015, Volume A, Theory and User Information, MSC.Software Corporation (2015)
- [21] J. Matějček, B. Nevrlá, J. Čech, M. Vilémová, V. Klevarová, and P. Haušild: Mechanical and thermal properties of individual phases formed in sintered tungsten-steel composites. *Acta Physica Polonica A* **128**, 718 (2015)
- [22] P. Haušild, A. Materna, L. Kocmanová, and J. Matějček: Determination of the individual phase properties from the measured grid indentation data. *J. Mater. Res.* **31**, 3538 (2016)
- [23] R.M. Christensen: Mechanics of composite materials. Wiley, New York (1979)
- [24] E. Lassner and W.-D. Schubert: Tungsten: properties, chemistry, technology of the element, alloys, and chemical compounds. Kluwer Academic/Plenum Publishers, New York (1999)
- [25] V. Brožek, P. Ctibor, J. Matějček, R. Mušálek, and Z. Weiss:

- Tungsten coatings and free standing parts. In Proc.: Metal 2013, 15.-17.5. 2013, Brno, Czech Republic, Tanger, 6 p. (2013)
- [26] CRC materials science and engineering handbook, 3rd ed. CRC press (2001)
- [27] D. Leisen, I. Kerkamm, E. Bohn, and M. Kamlah: A novel and simple approach for characterizing the Young's modulus of single particles in a soft matrix by nanoindentation. *J. Mater. Res.* **27**, 3073 (2012)

Curriculum vitae

Doc. Dr. Ing. Petr Haušild

Datum narození: 22. října 1975

Vzdělání, pedagogické a vědecké hodnosti:

2010 – doc. v oboru Fyzikální a materiálové inženýrství, ČVUT v Praze

2002 – Dr., Ecole Centrale Paris, Laboratoire de Mécanique de Sols, Structures et Matériaux

1999 – Mastère, Ecole Centrale Paris, Option: Science et génie des matériaux

1998 – Ing., České vysoké učení technické v Praze, Fakulta jaderná a fyzikálně inženýrská, Zaměření: Stavba a vlastnosti materiálů

Zaměstnání:

2010- Docent - Katedra materiálů, Fakulta jaderná a fyzikálně inženýrská, České vysoké učení technické v Praze

2002-2010 Odborný asistent - Katedra materiálů, Fakulta jaderná a fyzikálně inženýrská, České vysoké učení technické v Praze

1999-2002 Odborný asistent - Laboratoire de Mécanique Sols, Structures et Matériaux, Ecole Centrale Paris

1999-1999 Stážista - Electricité de France, Département d'Etudes des Matériaux Renardières

1996-1998 Pomocný vědecký pracovník - Katedra materiálů, Fakulta jaderná a fyzikálně inženýrská, České vysoké učení technické v Praze

Výzkumná činnost:

Materiálové inženýrství. Vědecko-výzkumná činnost v oboru fyzikální metalurgie, studium procesů porušování materiálů a výzkum vlastností nových materiálů. Analýza příčin poruch, fraktografická analýza, lokální elektronová mikroanalýza. Zkoušení mechanických vlastností materiálů.

Publikace:

Autor a spoluautor více než 50 článků v recenzovaných (impaktovaných) časopisech, více než 50 příspěvků ve sbornících z mezinárodních i tuzemských konferencí. Autor a spoluautor více než 100 výzkumných zpráv a expertíz.

Citace:

> 350 citací v databázi Web of Science, h-index(WoS) 13

Aplikační výstupy:

Spoluautor 6 funkčních vzorků, podíl na vývoji 4 certifikovaných metodik.

Členství:

European Microbeam Analysis Society (EMAS)

European Structural Integrity Society (ESIS)

Výzkumné projekty:

Řešitel, spoluřešitel nebo člen výzkumného týmu více než 20 výzkumných projektů GAČR, TAČR, MPO, MŠMT a ČVUT. V posledních 5 letech řešitel 1 standardního projektu GAČR, řešitel 1 rozvojového projektu MŠMT a garant 1 studentského výzkumného projektu ČVUT.

Vybrané granty:

1. Komplexní funkčně gradované materiály. Projekt GA ČR P108/12/1872 (2012-2014)
2. Vytvoření podmínek pro komplexní výuku magisterských a doktorských studentů se zaměřením na kovové materiály. Centrální rozvojový projekt MŠMT (2013)
3. Moderní technologie úpravy povrchů – Projekt ČVUT v Praze SGS 10/300/OHK4/3T/14 (2010-2012)

Výuka:

Stavba a vlastnosti materiálu, Nauka o materiálu pro reaktory, Fyzika kovů, Fyzikální metalurgie

Koncepce výuky v oboru Fyzikální a materiálové inženýrství:

Sledování moderních trendů v materiálovém inženýrství (vývoj nových materiálů, výrobních procesů, povrchových úprav atd.) a jejich začlenění do stávající výuky.

Zavedení výuky experimentálních metod umožňujících charakterizaci vlastností materiálu v mikro(nano)objemu jako jsou nanoindentace, DMA, FEG SEM, EBSD, XPS atd.

Propojení teoretické výuky s praktickými laboratorními cvičeními, při kterých studenti získají zkušenosti s prací na moderním přístrojovém vybavení.

Vybrané publikace:

- [1] Haušild, P. - Berdin, C. - Bompard, P. - Verdière, N.: Ductile Fracture of Duplex Stainless Steel with Casting Defects. *International Journal of Pressure Vessels and Piping*. 2001, vol. 78, no. 9, p. 607-616. ISSN 0308-0161.
- [2] Haušild, P. - Nedbal, I. - Berdin, C. - Prioul, C.: The Influence of Ductile Tearing on Fracture Energy in the Ductile-to-Brittle Transition Temperature Range. *Materials Science and Engineering A*. 2002, vol. 335, no. 1-2, p. 164-174. ISSN 0921-5093.
- [3] Nohava, J. - Haušild, P. - Karlík, M. - Bompard, P.: Electron Backscattering Diffraction Analysis of Secondary Cleavage Cracks in a Reactor Pressure Vessel Steel. *Materials Characterization*. 2002, vol. 49, no. 3, p. 211-217. ISSN 1044-5803
- [4] Haušild, P. - Berdin, C. - Bompard, P.: Prediction of Cleavage Fracture for a Low Alloy Steel in the Ductile-to-Brittle Transition Temperature Range. *Materials Science and Engineering A*. 2005, vol. 391, no. 1-2, p. 188-197. ISSN 0921-5093.
- [5] Strnadel, B. - Haušild, P.: Statistical Scatter in the Fracture Toughness and Charpy Impact Energy of Pearlitic Steel. *Materials Science and Engineering A*. 2008, vol. 486, no. 1-2, p. 208-214. ISSN 0921-5093.
- [6] Haušild, P. - Siegl, J. - Málek, P. - Šíma, V.: Effect of C, Ti, Zr and B Alloying on Fracture Mechanisms in Hot-Rolled Fe-40 (at.%)Al. *Intermetallics*. 2009, vol. 17, p. 680-687. ISSN 0966-9795.
- [7] Haušild, P. - Davydov, V. - Drahokoupil, J. - Landa, M. - Pilvin, P.: Characterization of Strain-induced Martensitic Transformation in a Metastable Austenitic Stainless Steel. *Materials and Design*. 2010, vol. 31, no. 4, p. 1821-1827. ISSN 0261-3069.
- [8] Skiba, T. - Haušild, P. - Karlík, M. - Vanmeensel, K. - Vleugels, J.: Mechanical Properties of Spark Plasma Sintered FeAl Intermetallics. *Intermetallics*. 2010, vol. 18, no. 7, p. 1410-1414. ISSN 0966-9795.
- [9] Haušild, P. - Materna, A. - Nohava, J.: On the identification of stress-strain relation by instrumented indentation with spherical indenter. *Materials and Design*. 2012, vol. 37, p. 373-378. ISSN 0261-3069.
- [10] Haušild, P. - Kolařík, K. - Karlík, M.: Characterization of Strain-Induced Martensitic Transformation in A301 Stainless Steel by Barkhausen Noise Measurement. *Materials and Design*. 2013, vol. 44, p. 548-554. ISSN 0261-3069.